J. Chem. Sci. (2021) 133:61
https://doi.org/10.1007/s12039-021-01917-2

REGULAR ARTICLE

Special Issue on Beyond Classical Chemistry

Substrate sulfoxidation by a biomimetic cytochrome P450 Compound I mimic: How do porphyrin and phthalocyanine equatorial ligands compare?

SAAID ROACH[a], ABAYOMI S FAPONLE[b], JAGNYESH KUMAR SATPATHY[c], CHIVUKULA V SASTRI[c] and SAM P DE VISSER[a,c,*]

[a]Department of Chemical Engineering and Analytical Science, Manchester Institute of Biotechnology, The University of Manchester, 131 Princess Street, Manchester M1 7DN, UK
[b]Department of Biochemistry, Faculty of Basic Medical Sciences, Olabisi Onabanjo University, Ago-Iwoye, Sagamu Campus, Ogun State, Nigeria
[c]Department of Chemistry, Indian Institute of Technology Guwahati, Guwahati, Assam 781 039, India
E-mail: sam.devisser@manchester.ac.uk; asfb340@yahoo.com; sastricv@iitg.ac.in

MS received 10 February 2021; revised 18 March 2021; accepted 22 March 2021

Abstract. The cytochrome P450 enzymes are important enzymes in the liver that trigger drug metabolism reactions. In biotechnology and biomimetic chemistry, synthetic models of the active species of P450 have been developed and designed and often react differently. Here, we investigate a biomimetic P450 model complex with phthalocyanine equatorial ligand rather than heme or porphyrin and with and without four *tert*-butyl substituents to the periphery of the ligand. Density functional theory studies on the electronic properties of the active species of the system, namely the iron(IV)-oxo with equatorial ligand cation radical species and its reactivity in oxygen atom transfer were studied. The work shows that a phthalocyanine equatorial ligand rather than porphyrin leads to a dramatic effect on the orbital energy levels of the iron(IV)-oxo species and creates a species with close-lying doublet and quartet spin states with two unpaired electrons in π^*_{xz} and π^*_{yz} for the Fe−O interaction coupled to a ligand radical in an a_{1u}-type orbital. The latter contrasts P450 Compound I that has the a_{1u} orbital doubly occupied and a singly occupied a_{2u} orbital instead, As a consequence, our biomimetic model gives a reduced redox potential as compared to a system with a porphyrin-based radical and makes it a weaker oxidant. Nevertheless, the iron(IV)-oxo cation radical species with phthalocyanine ligand is shown to react with *para*-X-substituted thioanisole (X = CH_3, Cl, CN, H, NO_2, OCH_3) substrates with small oxygen atom transfer barriers that align with the σ-Hammett parameter. The reactions are concerted with a single barrier leading to sulfoxide products.

Keywords. Biomimetic models; Density functional theory; Inorganic reaction mechanisms; Porphyrin; Iron.

1. Introduction

Heme enzymes are versatile catalysts in nature involved in the biosynthesis and biodegradation of compounds in biosystems.[1–9] As such, they function as peroxidases and catalases as well as mono-oxygenases. The latter group are labelled the cytochromes P450 and contain a heme-iron bound to the protein *via* a cysteinate group.[10,11] These P450 mono-oxygenases are found in the liver, where they participate in the degradation and metabolism of a variety of compounds, including drugs and xenobiotics.[12,13] In addition to this, they are also involved in the biosynthesis of hormones such as estrogen.[14,15] The P450 mono-oxygenases undergo a catalytic cycle that uses one molecule of O_2, two electrons and two protons to convert an iron(III)-heme into an iron(IV)-oxo heme cation radical species called Compound I (Cpd I).[16,17] Cpd I is known to react with substrates through oxygen atom transfer often in the form of aliphatic and aromatic hydroxylation, epoxidation, desaturation and sulfoxidation reactions.[18,19]

*For correspondence

Supplementary Information: The online version contains supplementary material available at https://doi.org/10.1007/s12039-021-01917-2.

Published online: 18 June 2021

Since P450 Cpd I is highly reactive and difficult to trap and characterize, many experimental efforts have been directed toward biomimetic model complexes that have the structural features of the oxidant in its first-coordination sphere, but lack the protein.[20–24] In particular, changes to the heme scaffold and replacing it with the structurally similar porphyrin, corrole, corrolazine or phthalocyanine ligands often changes the properties of the active oxidant and its reactivity patterns.[25–27] These studies have given insight into the chemical and functional properties of the heme group in heme enzymes and how the intricate design of the enzyme active site enables its high reactivity and selectivity.[28]

In this work, we focus on the structure and reactivity of iron-phthalocyanine complexes as shown in Scheme 1. Thus, experimental studies of Sorokin *et al.,*[29] characterized a biomimetic Cpd I species with tetra-*tert*-butyl-phthalocyanine equatorial ligand using UV-visible, electron paramagnetic resonance (EPR) and mass spectrometry techniques. These studies identified the iron(IV)-oxo species as a doublet spin ground state with unpaired spin density on the phthalocyanine ligand coupled to an iron radical. In addition, the same group prepared and characterized an *N*-bridged diiron oxo tetra(*tert*-butyl)phthalocyanine cation radical complex from the heterolytic O−O bond cleavage of the anionic diiron phthalocyanine hydroperoxo complex.[30] The intermediate was characterised by UV-visible, EPR, Mössbauer and X-ray absorption spectroscopies. This *N*-bridged diiron-oxo species was shown to be able to oxidize methane at ambient temperatures and react with benzene through oxygen-atom transfer.

In analogous studies, a high valent iron(IV)-oxo tetramesitylporphyrin (TMP) π-cation radical complex, i.e. a Cpd I mimic, was prepared and characterised by several spectroscopic techniques including UV-visible, NMR, EPR, Mössbauer, and resonance Raman spectroscopies.[31] Furthermore, the effect of the porphyrin structure and the electronic structure on the reactivity of iron(IV)-oxo porphyrin π-cation radical species was studied. Electron withdrawing substituents such as tetra-2,6-dichlorophenyl and tetra-pentafluorophenyl at the *meso* position of the porphyrin ring were shown to make the oxidant more effective for oxygen atom transfer reactions.[32] Subsequent studies of Fujii et al explored the iron(IV)-oxo porphyrin complex with substituents at the pyrrole β-position, i.e. 2,7,12,17-tetramethyl-3,8,13,18–tetramesitylporphyrin (TMTMP).[33] Drastic changes in the electronic states and magnetic properties of the complex were observed upon changes in the substitution patterns at the *β*-positions of the pyrrole rings as compared to the previously reported substitutions at the *meso*-position. The oxo iron porphyrin π-cation radical complexes with electron-withdrawing groups were shown to be more reactive as compared to the electron-donating substituents. The effect of the axial ligand on the structure and reactivity of the oxo iron(IV) porphyrin π-cation radical complexes was examined.[34] These studies were followed by a series of density functional theory (DFT) calculations on the effect of the axial ligands on the substrate sulfoxidation by an iron(IV)-oxo porphyrin cation radical species and showed that the barriers correlated with the ionization potential of the substrate and the electron affinity of the oxidant.[35]

Apart from studies on heme-containing iron complexes, there is a plethora of studies reported on biomimetic non-heme iron systems. In particular, these studies focused on the effects of metal-ligand distances,[36] electronic and steric comparisons,[37] axial ligation,[38] isolobal analogues[39] on the reactivity of iron(IV)-oxo metal complexes have been brought to the forefront over the years. As P450 enzymes typically catalyse substrate sulfoxidation reactions, often as part of a drug metabolism reactions,[40–42] it is often the reaction of choice for model reactions. The effect of sulfoxidation of *para*-substituted thioanisole by a non-heme iron(IV)-oxo complex with N4Py (*N*,*N*-bis(2-pyridylmethyl)-*N*-bis(2-pyridyl) methylamine) ligand was investigated.[43] Detailed computational studies on the sulfoxidation of sulphides by this iron(IV)-oxo complex was conducted by us and rationalized with valence bond schemes.[44–46] Interestingly, a mechanistic switch from sulfoxidation of thioanisole by non-heme iron(IV)-oxo to simple

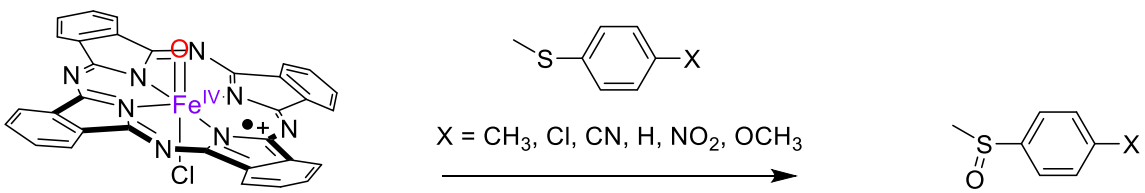

Scheme 1. Iron-phthalocyanine complex [Fe^{IV}(O)(Pc$^{+\bullet}$)(Cl)] and its reactivity with *para*-X-substituted thioanisole substrates.

oxygen-atom transfer to the metal ion-coupled electron transfer (MCET) was observed in the presence of Sc^{3+}.[47] Also, upon the addition of Sc^{3+}, the rate of the sulfoxidation reaction increased by 100 fold. Similarly, the addition of triflic acid (HOTf) and $Sc(OTf)_3$ during the sulfoxidation reaction rendered proton-coupled electron transfer (PCET) and MCET as the driving forces.[48] In addition, studies with various tetradentate and pentadentate iron(IV)-oxo complexes highlighted major differences in reactivity and spectroscopic properties.[49] To understand the equatorial ligand effect of iron(IV)-oxo species better, we did a detailed computational study on the biomimetic P450 Cpd I model with phthalocyanine equatorial ligand. The work shows that this system has an unusual electronic configuration that should weaken its oxidative properties; although, it should be able to react with sulphides via oxygen atom transfer.

2. Experimental

2.1 *Model set-up*

We created an iron(IV)-oxo models with phthalocyanine (Pc) ligand based on computational structures published previously.[50–52] These models were validated against experiment and shown to be good mimics of the actual system. Model **A** is the bare system with all phthalocyanine substituents abbreviated by hydrogen atoms and with chloride as the axial ligand, i.e. [Fe^{IV}(O)($Pc^{+\bullet}$)(Cl)]. This system is overall charge-neutral and was calculated in the doublet and quartet spin states. Chloride was chosen as the axial ligand ion as it is isoelectronic to sulphide in its bound form and therefore is a good mimic of the enzymatic system.[53]

Despite the fact that previous work showed little effect of substituents on the periphery of porphyrinoid systems,[54,55] we tested a second and more elaborate model based on model **A** but with four *t*-Bu substituents on the periphery of the phthalocyanine ring (model **B**), i.e. [Fe^{IV}(O)($PcBu^{+\bullet}$)(Cl)].

The reactivity of model **A** and **B** with the substrate was tested with various *para*-X-thioanisole (X = Me, Cl, CN, H, NO_2, OMe) for substrate sulfoxidation.

2.2 *Computational methods and design*

The structure and reactivity of complexes **A** and **B** were studied with density functional theory methods as implemented in the *Gaussian*-09 software package.[56] In general, the unrestricted hybrid density functional method B3LYP[57,58] was used in combination with a LACVP basis set (with core potential) on iron and 6-31G* on the rest of the atoms (basis set BS1) for geometry optimizations of local minima and transition states, analytical frequency calculations and constraint geometry scans.[59–61] To correct the energies, single-point calculations with the LACV3P+ basis set on iron (with core potential) and 6-311+G* on the rest of the atoms (basis set BS2) was performed. These single-point calculations also included the continuum polarized conductor model with a dielectric constant mimicking acetone. Free energies are reported at 298 K and 1 atm and used unscaled vibrational frequencies.

Initially models **A** and **B** were geometry optimized in the gas phase at UB3LYP/BS1, but some test calculations were done with geometry optimizations that include a solvent model: structures **As** and **Bs**.

The methods used in this work have been extensively used in our groups and shown to reproduce experimental free energies of activation to within 3 kcal mol^{-1}.[62–65] Moreover, the methods for analogous problems were shown to correctly reproduce experimental selectivities and product distributions.[66–69]

3. Results and Discussion

We started with a series of geometry optimizations on the iron(IV)-oxo phthalocyanine cation radical complexes [Fe^{IV}(O)($Pc^{+\bullet}$)(Cl)] and [Fe^{IV}(O)($PcBu^{+\bullet}$)(Cl)] with and without a solvent model included in the calculations. Optimized geometries of ^{4,2}**A**, ^{4,2}**B**, ^{4,2}**As** and ^{4,2}**Bs** are shown in Figure 1. As can be seen, enlarging the model with four *tert*-Bu substituents on the periphery of the phthalocyanine ligand has very little effect on the Fe−O, Fe−Cl and Fe−N bond lengths and all of those change by less than 0.005 Å. In all cases, the Fe−O distance is short: 1.64 Å in the gas phase and 1.63 Å with a solvent model included. These Fe−O distances match previous calculations on Cpd I of P450 and biomimetic iron(IV)-oxo porphyrin complexes.[70–80] Moreover, experimentally observed Fe−O distances on biomimetic Cpd I model complexes (both heme and non-heme) were found to be ranging between 1.62 and 1.67 Å;[81–86] and hence, are of similar magnitude to the results obtained here. In the case of cytochrome *c* peroxidase and cytochrome P450, the bond lengths are even further extended up to 1.7−1.9 Å and 1.65 Å, respectively, although the former may correspond to a reduced or protonated species instead. Similarly, the distances observed for the non-heme model systems containing ligand

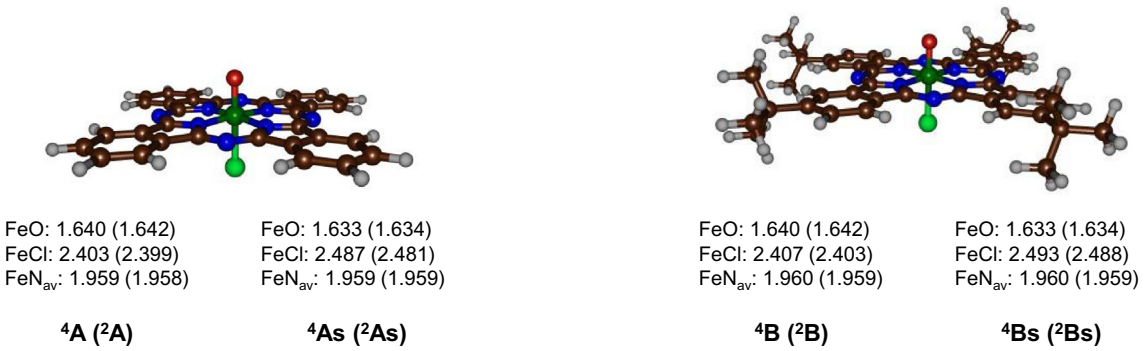

Figure 1. Optimized geometries of iron(IV)-oxo phthalocyanine cation radical complexes in the gas phase (models **A/B**) and with a solvent model included (models **As/Bs**). Bond lengths are in angstroms.

frameworks like TMC (TMC = 1,4,8,11-tetramethyl-1,4,8,11-tetraazacyclotetradecane) and N4Py are 1.646 and 1.64 Å, respectively. It appears; therefore, that the iron(IV)-oxo phthalocyanine cation radical is structurally similar to analogous porphyrin complexes, which would not explain the reactivity differences between the two systems.

To understand the electronic properties of the iron(IV)-oxo reactant complexes, we analysed the molecular orbitals in detail. Figure 2 displays the high-lying valence orbitals of typically seen in **A**, **B**, **As** and **Bs**. These orbitals take the z-axis along the Fe−O bond and the x- and y-axis in the phthalocyanine plane and in between two Fe−N bonds. There are five orbitals with metal 3d contributions that are labelled according to the 3d orbital of iron that is involved. The lowest in energy and doubly occupied in all structures is the $\delta_{xx\text{-}yy}$ orbital in the plane of the phthalocyanine group and is nonbonding. Higher in energy and singly occupied in the reactant complexes are the π*-type interactions of the metal $3d_{xz}$ and $3d_{yz}$ orbitals with a 2p orbital on the oxo group in the same plane. In the reactant states the σ* orbitals are virtual and represent the interactions along the Cl−Fe−O axis (σ^*_{zz}) and in the plane of the phthalocyanine between the iron and nitrogen atoms (σ^*_{xy}). There are also a number of π*-type phthalocyanine-based orbitals and two of those are shown on the right-hand side of Figure 2, namely the a_{1u} and a_{2u} orbitals. In P450 Cpd I, the a_{2u} orbital is singly occupied and is filled during the substrate

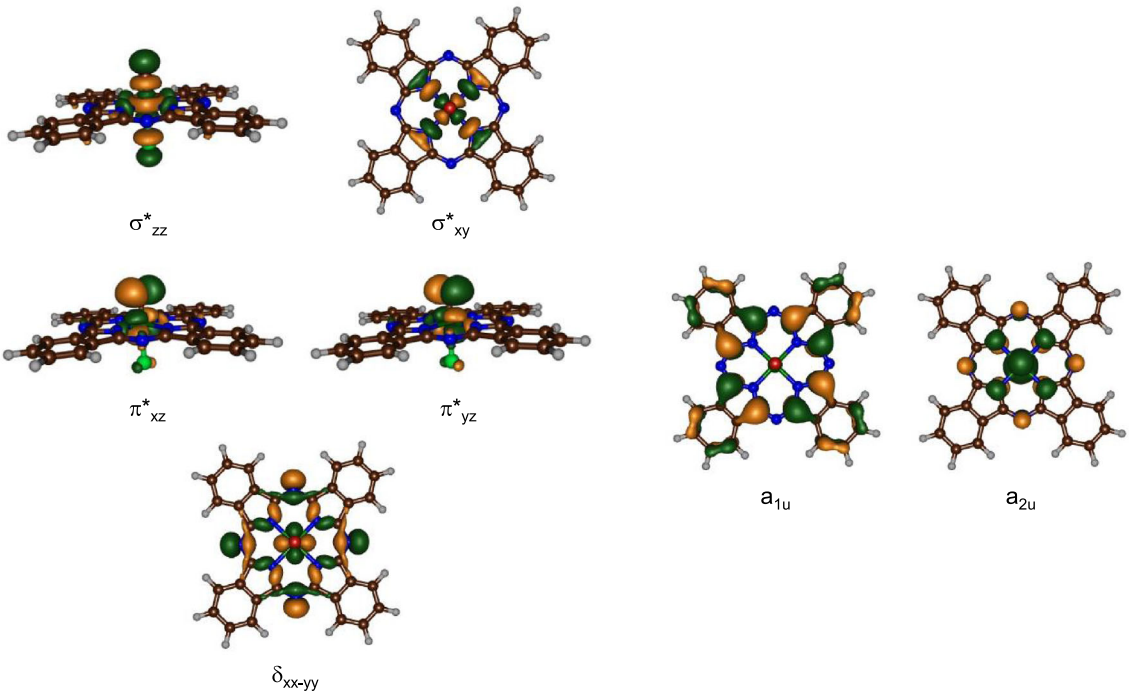

Figure 2. Molecular valence orbitals of iron(IV)-oxo phthalocyanine cation radical complexes in the gas phase (models **A/B**) and with a solvent model includes (models **As/Bs**). Examples are shown of the orbitals of structure **A**.

activation reaction mechanism.[16–19,87,88] Hence, the electron affinity of the heme is an important factor in P450 reactivity.

The orbitals shown in Figure 2 are occupied with seven electrons and give an electronic ground state for **A**, **B**, **As** and **Bs** of $\delta_{xx\text{-}yy}^{2}\pi^{*}_{xz}{}^{1}\pi^{*}_{yz}{}^{1}$ $a_{2u}{}^{2}$ $a_{1u}{}^{1}$, whereby the a_{1u} electron is down-spin in the doublet spin state and up-spin in the quartet spin state. This electronic ground state is different from that found in P450 Cpd I and biomimetic iron(IV)-oxo porphyrin cation radical complexes that always give an a_{2u} radical and no a_{1u} radical.[70–80] As a matter of fact, a DFT study on a small iron(IV)-oxo complex in the gas phase gave an energy gap between the states with a_{2u} and a_{1u} singly occupied of well over 20 kcal mol^{-1}.[70,73] We attempted to swap molecular orbitals for all structures but in all cases, the SCF converged back to a state with a singly occupied a_{1u} orbital. As such, the electronic configuration with the a_{1u} orbital singly occupied is the ground state and well lower in energy than the one with a_{2u} singly occupied with a phthalocyanine ligand. Interestingly, for a manganese(V)-oxo corrolazine cation radical system, Goldberg et al also found the a_{1u}-type orbital higher in energy and singly occupied with the a_{2u}-type orbital doubly occupied.[89] Therefore, replacing the *meso*-carbon atom in porphyrin with a *meso*-nitrogen atom as in phthalocyanines changes the π-type orbitals on the equatorial ligand and brings the a_{2u}-type orbital below the a_{1u}-type orbital in energy. This also must affect the redox potential of the equatorial ligand and consequently its reactivity with substrates.

Subsequently, we investigated the reactivity of complexes **A** and **B** towards oxygen atom transfer to sulphides and used *para*-X-substituted thioanisole as a model. All reactions are concerted with a single oxygen atom transfer to form sulfoxide products, which is similar to previous substrate sulfoxidation reactions reported by P450 and model systems.[35,90] The quartet spin state structures are the lowest in energy and well lower than the corresponding doublet spin state structures. The ordering is similar to those of the product complexes that also have the quartet spin structures well below the doublet spin. As such we will focus on the quartet spin structures only. Optimized geometries of the quartet spin oxygen atom transfer transition states ($\mathbf{TS}_{SO,As,X}$) for model **As** are given in Figure 3. In all structures the Fe−O bond has elongated with respect to the reactant complex to values ranging from 1.799–1.813 Å and hence all structures fall in a narrow window. A bit more fluctuation is seen in the Fe−Cl interaction that is only 2.539 Å in $^{4}\mathbf{TS}_{SO,As,NO2}$, while it is somewhat longer in $^{4}\mathbf{TS}_{SO,As,Me}$ at 2.670 Å. As the sulfoxidation process involves an electron transfer into the σ^{*}_{zz} molecular orbital that is located along the O−Fe−Cl bond, this means both Fe−O and Fe−Cl distances elongate.

The sulfoxidation transition states are characterized with relatively large imaginary frequencies for the S−O stretch vibration with values that range from i554 cm^{-1} for $^{4}\mathbf{TS}_{SO,As,NO2}$ to i733 cm^{-1} for $^{4}\mathbf{TS}_{SO,As,H}$. These structures have an S−O interaction that follows the trend of the imaginary frequencies with a small distance of 1.928 Å for $^{4}\mathbf{TS}_{SO,As,NO2}$ and the longest distance for $^{4}\mathbf{TS}_{SO,As,OMe}$ with a value of 2.039 Å. We also optimized the transition states for the large model **Bs** and those structures are given in Figure 4. Most distances are very similar between models **As** and **Bs** and so are the imaginary frequencies in the transition states. Clearly, the addition of *tert*-Bu groups to the periphery of the phthalocyanine ligand has little effect on the structure and reactivity with substrates.

The energetics of the substrate sulfoxidation barriers of models **As** and **Bs** are given in Table 1 as well as the corresponding σ Hammett parameters for the *para*-substituent.[91] In general, we find the same trends whether enthalpies (ΔE+ZPE) or free energies (ΔG) are used. Moreover, changing the model with four additional *tert*-Bu substituents on the periphery of the phthalocyanine ligand has a small effect and generally lifts the barriers systematically by a few kcal mol^{-1}. The addition of entropy and thermal corrections to the enthalpies gives a change in the numbers of about 12 kcal mol^{-1} for all structures and systems are shown in Table 1. Although it should be mentioned that gas-phase DFT calculations often overestimate entropy contributions and sometimes by as much as 50%.[46]

Next, we analysed the substrate sulfoxidation transition state energies and plotted those for the reaction of **As** with para-X-substituted thioanisole (X = OCH_3, CH_3, H, Cl, CN, NO_2) against the σ-Hammett parameter and show the trends in Figure 5. [78] As can be seen, whether relative energies of free energies are used, a reasonably linear correlation with the σ-Hammett parameter is obtained. Relative energies (at ΔE+ZPE level of theory) range from 8.91 kcal mol^{-1} for $^{4}\mathbf{TS}_{SO,As,OMe}$ to 13.42 kcal mol^{-1} for $^{4}\mathbf{TS}_{SO,As,NO2}$ and as such cover a range of 4.5 kcal mol^{-1}. We also calculated the transition states for the large model with four additional *tert*-Bu groups on the periphery of the phthalocyanine ligand and its trend is shown on the right-hand-side of Figure 5. The trend is not as nice as for the bare system, probably due to interactions of the approaching substrate with the equatorial ligand system, but a small increasing trend is seen.

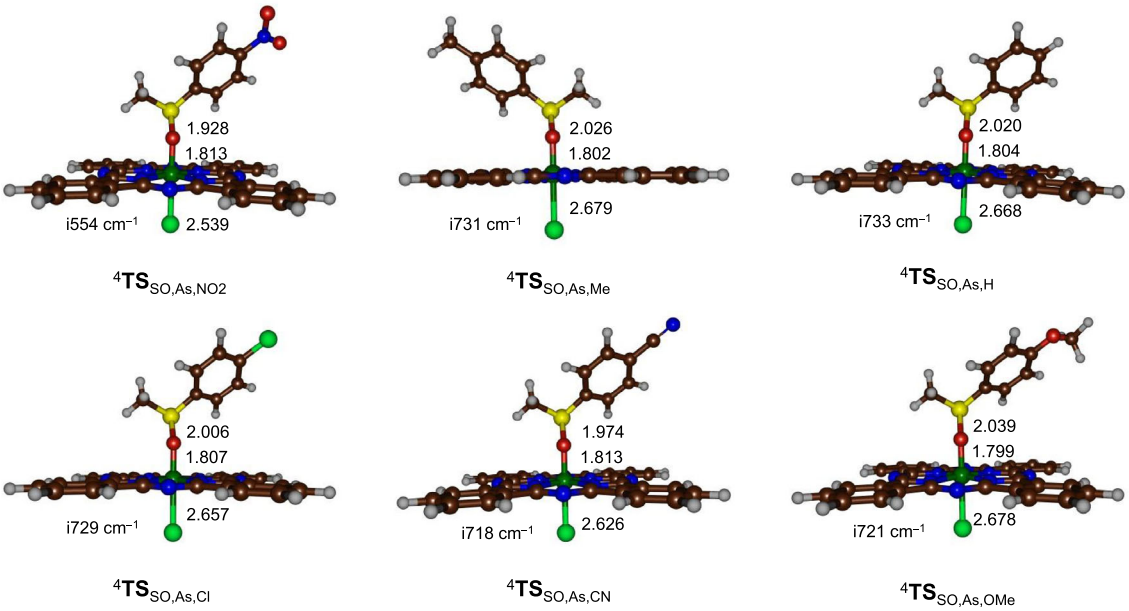

Figure 3. UB3LYP/BS1 optimized sulfoxidation transition states as obtained for model **As**. Bond lengths are in angstroms and the imaginary frequencies in cm^{-1}.

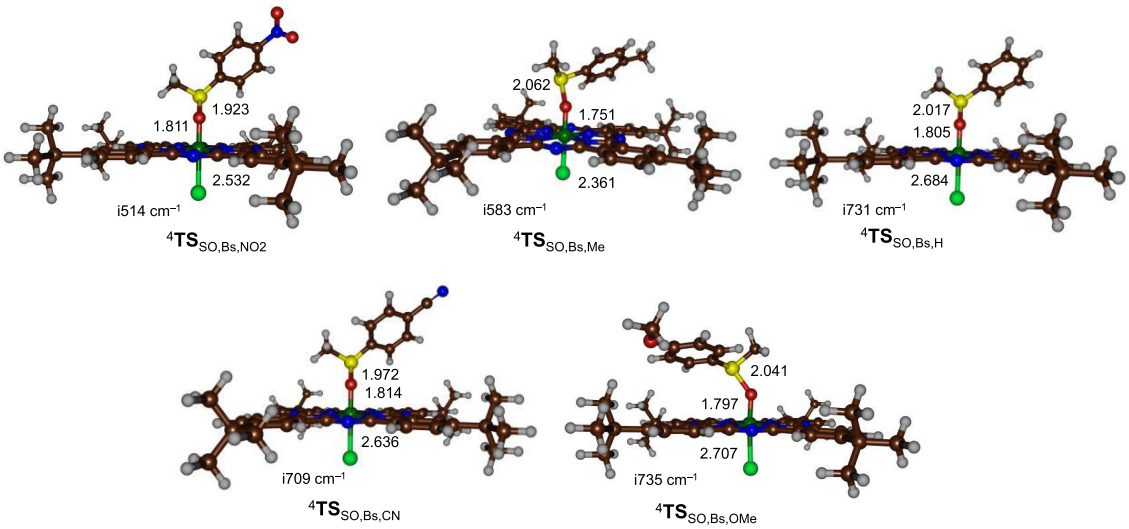

Figure 4. UB3LYP/BS1 optimized sulfoxidation transition states as obtained for model **Bs**. Bond lengths are in angstroms and the imaginary frequencies in cm^{-1}.

Overall, the DFT calculations on the reaction of **As** and **Bs** with *para*-X-substituted thioanisole give barriers that are close in energy and a small increase of the free energy of activation with a decrease in Hammett parameter. Whether the trends in Figure 5 mean that there is no effect of the *para*-substituent (flat curve) or there is a small increase cannot be determined at this stage as the margin may be within the error of the calculations. Therefore, experimental studies will be needed to be performed to confirm this trend. Nevertheless, it appears the effect of the *para*-substituent in the biomimetic Compound I models studied here may be considerably smaller than that seen in, e.g. nonheme iron(IV)-oxo oxidants. Thus, previous studies on substrate sulfoxidation by a nonheme iron(IV)-oxo species gave an increasing trend with increasing Hammett parameter in analogy with experimental studies.[92,93] In nonheme iron chemistry, the sulfoxidation reaction is accompanied with double electron transfer into the iron system, whereas in our system here, only one electron moves to the iron while the second one moves to the equatorial ligand. Also, studies on para-X-substituted

Table 1. Relative energies and free energies of *para*-X-substituted thioanisole sulfoxidation by models As and Bs in the quartet spin state.

		Model **As**		Model **Bs**	
X	σ^a	ΔE+ZPE	ΔG	ΔE+ZPE	ΔG
OCH_3	− 0.27	8.91	20.28	11.58	23.67
CH_3	− 0.17	9.27	21.29	17.31	29.56
H	0.00	10.62	21.35	12.39	23.43
Cl	0.23	11.07	21.94	ND	ND
CN	0.66	12.72	23.86	14.64	26.12
NO_2	0.78	13.42	25.21	15.37	27.12

Energies in kcal mol^{-1} relative to isolated reactants; ND = not determined.

[a]Hammett parameter taken from Ref.[91].

styrene epoxidation by an iron(IV)-oxo porphyrin cation radical gave linear trends of the free energy of activation against the substrate ionization potential.[94] The latter studies used a minimal model in the gas phase without substituents on the periphery. It may very well be that interactions of the second coordination sphere affect the trends as studied here.

To understand the electron transfer processes in the substrate sulfoxidation processes in the doublet and quartet spin states, we show the orbital occupation levels for the reactant (^{4,2}**Re**) and product (^{4,2}**Pr**) complexes in Scheme 2. As discussed above in Figure 2 the reactants have electronic configuration $\delta_{xx\text{-}yy}{}^2\pi^*_{xz}{}^1\pi^*_{yz}{}^1 a_{2u}{}^2 a_{1u}{}^1$ with the a_{1u} electron either with up-spin in the quartet spin state or down-spin in the doublet spin state. During the substrate sulfoxidation process, two electrons are transferred from substrate to oxidant. The first electron regardless of the overall spin-state will move into the a_{1u} orbital and make it closed-shell. In the doublet spin state the second electron is transferred into the π^*_{xz} orbital and fill it with two electrons, whereas in the quartet spin state the electron moves into the virtual σ^*_{zz} orbital. Although in porphyrin systems, the iron(III) complexes, such as the resting state in the catalytic cycle of P450 is in a doublet spin ground state,[5–9,17,19] the sulfoxidation reaction often takes place on a dominant quartet spin state surface.[35,90,95] Our studies with the phthalocyanine model; therefore, follow spin-state ordering and reactivity patterns analogous to related systems studied previously.

To understand whether the transition states have an electronic configuration closer to the reactants or products state, we analysed the molecular orbitals of the transition states and the group spin densities and charges. Figure 6 displays the spin densities of the ^{4}**TS**$_{SO,As,X}$ sulfoxidation transition states. As can be seen the structures have a spin of 1.6 (^{4}**TS**$_{SO,As,NO2}$) or 1.8 (all other transition states) on the FeO group, which implies that all structures have almost two unpaired electrons along the Fe–O bond. In addition, all structures keep a spin of 0.9 on the phthalocyanine ligand. Based on the comparison of the spin density data of Figure 6 and the electron transfer pathways in Scheme 2, it, therefore, follows that the transition states are early on the potential energy landscape and have an electronic configuration close to the reactant state. Moreover, the spin densities show that the two-electron transfer process in the sulfoxidation reaction happens sequentially, whereby the first electron transfer happens in the transition state, while the second one en route from the transition state to the product complex. We were not able to find a local minima for a one-electron transfer reaction and the geometry scans gave a direct collapse to the product complexes. As such, the second electron transfer in the sulfoxidation reaction is fast and occurs rapidly as soon as the S−O bond is formed.

Often the reactivity of metal-oxo complexes is correlated with thermochemical properties of the

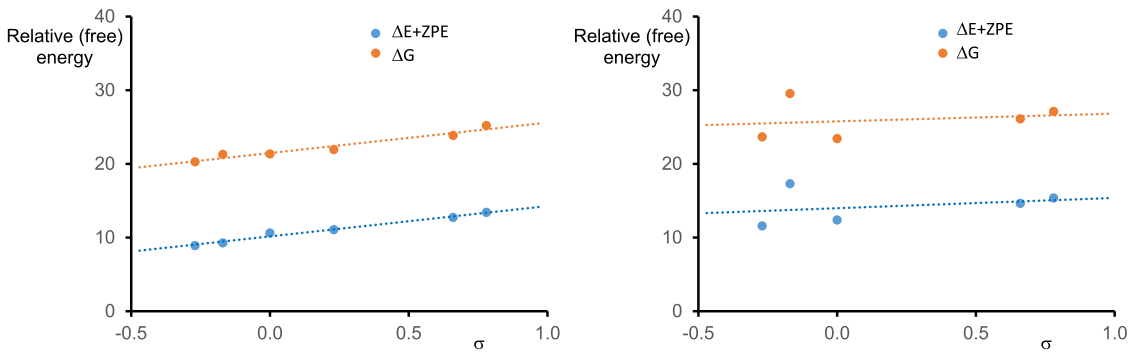

Figure 5. Relative energies and free energies of sulfoxidation transition states for *para*-X-substituted thioanisole with phthalocyanine model **As** (left-hand-side) and **Bs** (right-hand-side) as a function of the σ-Hammett parameter.

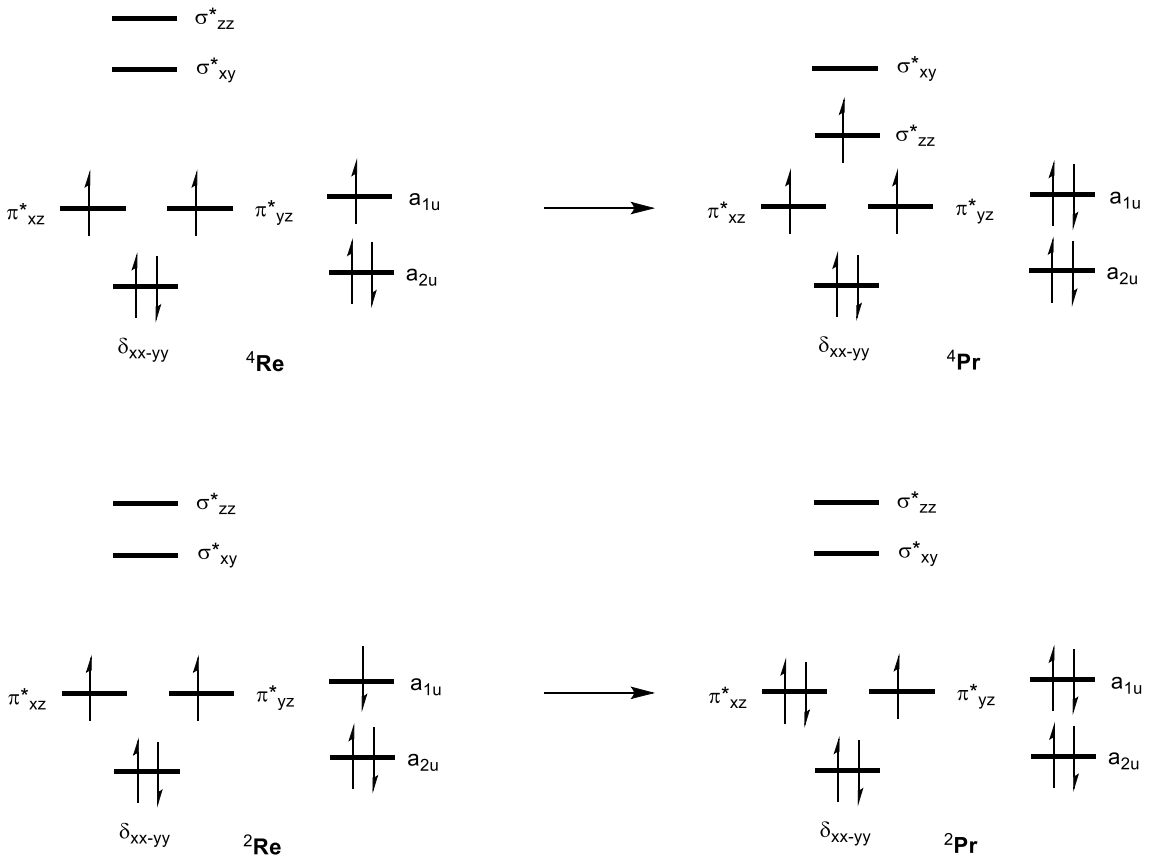

Scheme 2. Orbital occupation changes from reactants to products in the quartet (top) and doublet (bottom) spin states.

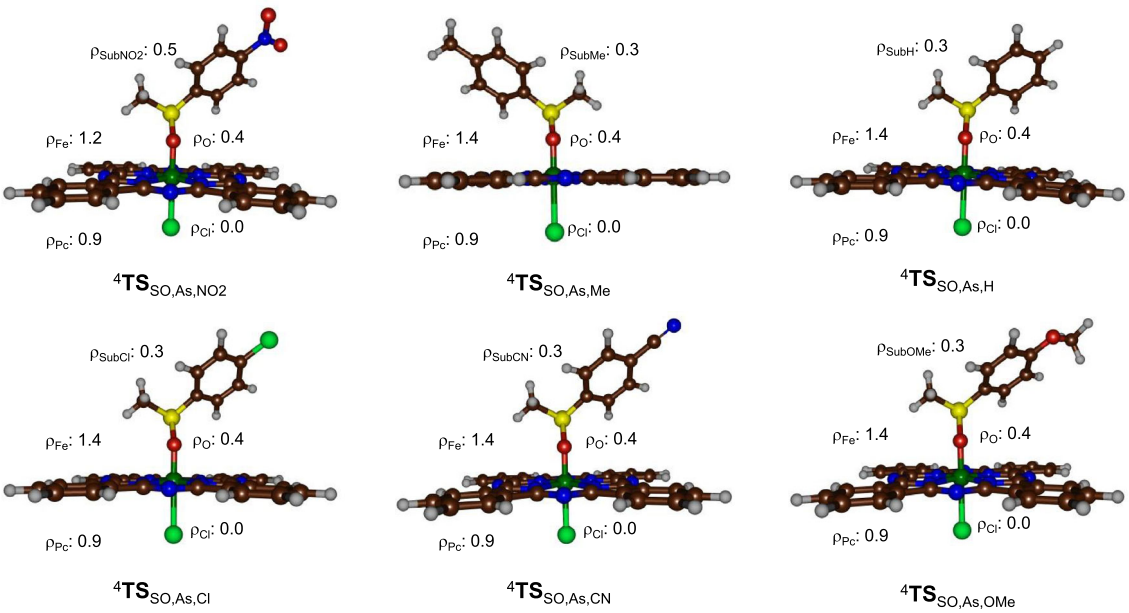

Figure 6. Group spin densities (ρ) of UB3LYP/BS1 optimized sulfoxidation transition states as obtained for model **As**.

oxidant, such as the one-electron electron affinity (EA) of the iron(IV)-oxo species and the O−H bond dissociation energy (BDE) of the iron(III)-hydroxo species.[35,80,88,96–104] Thus, the EA is defined as the adiabatic energy difference between [Fe^{IV}(O)($Pc^{+\bullet}$)(-Cl)] and its one-electron reduced structure, namely

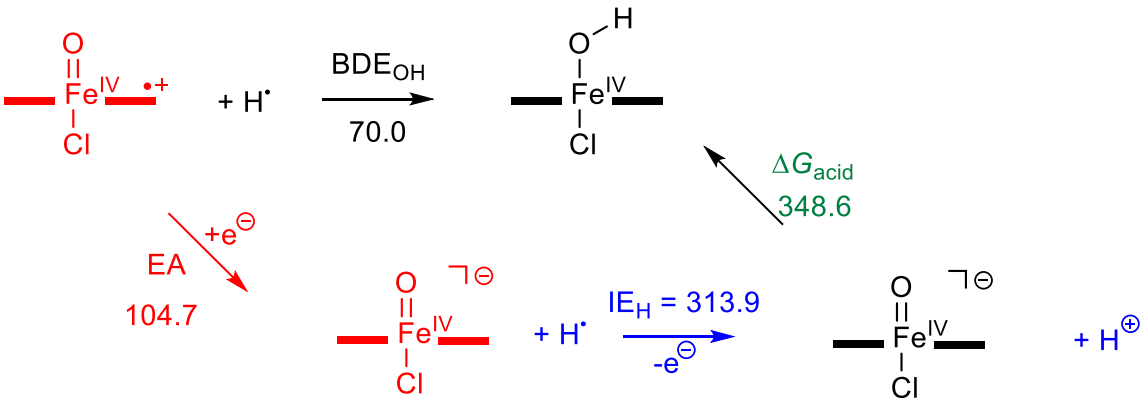

Figure 7. Thermochemical cycle for the iron(IV)-oxo phthalocynine model investigated here. Energies are in kcal mol^{-1} and represent ΔE+ZPE data. The value of IEH is taken from Ref[99].

[Fe^{IV}(O)(Pc)(Cl)]$^{-}$. Similarly, the energy of [Fe^{IV}(O)(Pc$^{+\bullet}$)(Cl)] to abstract a hydrogen atom to form [Fe^{IV}(OH)(Pc)(Cl)] is calculated from the energy difference of these structures. The thermodynamic cycle shown in Figure 7 also includes the gas-phase acidity of the iron-hydroxo complex, which is calculated from the EA and BDE values and the ionization energy (IE$_H$) of an isolated hydrogen atom. The latter was taken from the experimental data from the NIST database.[99]

Previously, it was shown that for substrate hydroxylation reactions by metal-oxo complexes with a rate-determining hydrogen atom abstraction step, the corresponding rate constant correlates with the C−H bond energy (BDE$_{CH}$) of the bond that is broken.[96,97] In particular, experimental work for several models showed that the natural logarithm of the rate constant of a hydrogen atom abstraction reaction is linearly proportional to BDE$_{CH}$. Computational studies confirmed these trends and showed that for a range of oxidants with the same substrate, the rate constant also correlates with the O−H bond strength of the iron-hydroxo complex that is formed in the process.[97] Furthermore, in substrate epoxidation and sulfoxidation reactions the formation of the rate-determining O−C and O−S bonds could be mimicked with an O−H bond and hence their rate constants also showed a correlation with BDE$_{OH}$.[35,98] Therefore, we evaluated the BDE$_{OH}$ value of [Fe^{IV}(O)(Pc$^{+\bullet}$)(Cl)] and compared its value with those obtained with analogous iron(IV)-oxo-porphyrin and nonheme iron(IV)-oxo complexes from the literature.

The calculated EA for [Fe^{IV}(O)(Pc$^{+\bullet}$)(Cl)] is 104.7 kcal mol^{-1}, while its BDE$_{OH}$ is 70.0 kcal mol^{-1}. From the cycle shown in Figure 7 using the experimental ionization energy of a hydrogen atom of IE$_H$ = 313.9 kcal mol^{-1}, we calculated a gas-phase acidity for the reduced iron(IV)-oxo species of ΔG$_{acid}$ = 348.6 kcal mol^{-1}. The BDE$_{OH}$ that was calculated for a P450 Cpd I model was 87.4 kcal mol^{-1}, which is considerably larger than the value obtained for the phthalocyanine system. This is probably the result of the higher energy a_{2u} orbital in P450 Cpd I that makes electron abstraction easier than in the phthalocyanine system and hence will create a stronger O−H bond formation step. As a consequence, the phthalocyanine system will be a weaker oxidant than an analogous porphyrin system and likely react with substrates with substantially higher reaction barriers. Indeed, for ethylphenylsulfide sulfoxidation by a P450 Cpd I model [Fe^{IV}(O)(Por)(Cl)] Kumar *et al.,* found a barrier of only 7.9 kcal mol^{-1},[35] while in this work all thioanisole sulfoxidation barriers by the phthalocyanine system are at least several kcal mol^{-1} higher in energy. Also a study on the sulfoxidation of para-X-substituted thioanisole by several nonheme iron(IV)-oxo complexes gave low barriers for all systems; however, those studies identified a small upward slope in the Hammett plot in agreement with experimental data. It appears that for the system studied here the Hammett plot has a much smaller slope. The porphyrin complex reported in reference[35] had a much larger electron affinity of around 120 kcal mol^{-1} and hence will abstract electrons much easier than the phthalocyanine system discussed here. The amount of charge transfer in the transition states will affect the slope of the Hammett plots.

4. Conclusions

A computational study is presented on the properties and reactivity of an iron(IV)-oxo phthalocyanine system with chloride axial ligand. The work shows that in contrast to an analogous P450 Cpd I system the

electronic ground state has three unpaired electrons in π^*_{xz}, π^*_{yz} and a_{1u} molecular orbitals. The latter gives the $[Fe^{IV}(O)(Pc^{+\bullet})(Cl)]$ system a weaker electron affinity and also a lower BDE_{OH} value. Subsequent studies on *para*-X-thioanisole sulfoxidation were done and showed these reactions to be concerted with a single oxygen-atom transfer leading to sulfoxides. Overall, the calculations predict that the iron(IV)-oxo phthalocyanine system should react with sulphides through oxygen-atom-transfer reactions. However, the calculated barriers are somewhat higher in energy than analogous nonheme iron(IV)-oxo and biomimetic Cpd I systems.

Acknowledgements

CVS acknowledges research support provided by the Department of Science and Technology (SERB), India through Grant code CRG/2019/000387. SPdeV and CVS thank the British Council for a UK-India Education and Research Initiative Grant (Grant code DST/INT/UK/P-151/2017). SPdeV thanks IIT Guwahati for a visiting professorship.

References

1. Sono M, Roach M P, Coulter E D and Dawson J H 1996 Heme-containing oxygenases *Chem. Rev.* **96** 2841
2. Ortiz de Montellano P R (Ed.) 2005 *Cytochrome P450: Structure, Mechanism and Biochemistry* 3rd edn. (Kluwer Academic/Plenum Publishers: New York)
3. Kadish K M, Smith K M and Guilard R (Eds.) 2010 *Handbook of Porphyrin Science* (World Scientific: New Jersey)
4. Munro A W, Girvan H M and McLean K J 2007 Variations on a (t)heme—novel mechanisms, redox partners and catalytic functions in the cytochrome P450 superfamily *Nat. Prod. Rep.* **24** 585
5. Ortiz de Montellano P R 2010 Hydrocarbon hydroxylation by cytochrome P450 enzymes *Chem. Rev.* **110** 932
6. Meunier B, de Visser S P and Shaik S 2004 Mechanism of oxidation reactions catalyzed by cytochrome P450 enzymes *Chem. Rev.* **104** 3947
7. Denisov I G, Makris T M, Sligar S G and Schlichting I 2005 Structure and chemistry of cytochrome P450 *Chem. Rev.* **105** 2253
8. Huang X and Groves J T 2018 Oxygen activation and radical transformations in heme proteins and metalloporphyrins *Chem. Rev.* **118** 2491
9. de Visser S P and Kumar D (Eds.) 2011 *Iron-containing enzymes: Versatile catalysts of hydroxylation reactions in nature*(Royal Society of Chemistry Publishing: Cambridge)
10. Schlichting I, Jung C and Schulze H 1997 Crystal structure of cytochrome P-450cam complexed with the (1S)-camphor enantiomer *FEBS Lett.* **415** 253
11. Poulos T L 2014 Heme enzyme structure and function *Chem. Rev.* **114** 3919
12. Taxak N and Bharatam P V 2010 An insight into the concept and details of mechanism-based inhibition of CYP450 *Curr. Res. Inform. Pharm. Sci.* **11** 62
13. Dixit V A, Lal L A and Agrawal S R 2017 Recent advances in the prediction of non-CYP450-mediated drug metabolism *Wiley Interdiscip. Rev.-Comput. Mol. Sci.* **7** e1323
14. Guengerich F P 2008 Cytochrome P450 and chemical toxicology *Chem. Res. Toxicol.* **21** 70
15. Bagha U K, Satpathy J K, Mukherjee G, Sastri C V and de Visser S P 2021 A comprehensive insight into aldehyde deformylation: mechanistic implications from biology and chemistry *Org. Biomol. Chem.* **19** 1879
16. Green M T 2009 C-H bond activation in heme proteins: the role of thiolate ligation in cytochrome P450 *Curr. Opin. Chem. Biol.* **13** 84
17. Dubey K D and Shaik S 2019 Cytochrome P450: The wonderful nanomachine revealed through dynamic simulations of the catalytic cycle *Acc. Chem. Res.* **52** 389
18. Huang X and Groves J T 2017 Beyond ferryl-mediated hydroxylation: 40 years of the rebound mechanism and C-H activation *J. Biol. Inorg. Chem.* **22** 85
19. Shaik S, Kumar D, de Visser S P, Altun A and Thiel W 2005 Theoretical perspective on the structure and mechanism of cytochrome P450 enzymes *Chem. Rev.* **105** 2279
20. Atanasov M, Comba P, Hausberg S and Martin B 2009 Cyanometalate-bridged oligonuclear transition metal complexes-Possibilities for a rational design of SMMs *Coord. Chem. Rev.* **253** 2306
21. Costas M 2011 Selective C-H oxidation catalyzed by metalloporphyrins *Coord. Chem. Rev.* **255** 2912
22. Barry S M, Mueller-Bunz H and Rutledge P J 2012 Investigating the oxidation of alkenes by non-heme iron enzyme mimics *Org. Biomol. Chem.* **10** 7372
23. Ray K, Pfaff F F, Wang B and Nam W 2014 Status of reactive non-heme metal-oxygen intermediates in chemical and enzymatic reactions *J. Am. Chem. Soc.* **136** 13942
24. Oloo W N and Que L Jr 2015 Bioinspired non-heme iron catalysts for C−H and C=C bond oxidation: Insights into the nature of the metal-based oxidants *Acc. Chem. Res.* **48** 2612
25. Baglia R A, Zaragoza J P T and Goldberg D P 2017 Biomimetic reactivity of oxygen derived manganese and iron porphyrinoid complexes *Chem. Rev.* **117** 13320
26. Haviv-Arel I and Gross Z 2011 Coordination chemistry of corroles with focus on main group elements *Coord. Chem. Rev.* **255** 717
27. Sorokin A B 2013 Phthalocyanine metal complexes in catalysis *Chem. Rev.* **113** 8152
28. de Visser S P 2020 Second-coordination sphere effects on selectivity and specificity of heme and nonheme iron enzymes *Chem. Eur. J.* **26** 5308

29. Afanasiev P, Kudrik E V, Albrieux F, Briois V, Koifman O I and Sorokin A B 2012 Generation and characterization of high-valent iron oxo phthalocyanines *Chem. Commun.* **48** 6088
30. Afanasiev P, Kudrik E V, Millet J M M, Bouchu D and Sorokin A B 2011 High-valent diiron species generated from N-bridged diiron phthalocyanine and H_2O_2 *Dalton Trans.* **40** 701
31. Groves J T, Haushalter R C, Nakamura M, Nemo T E and Evans B J 1981 High valent iron-porphyrin complexes related to peroxidase and cytochrome P-450 *J. Am. Chem. Soc.* **103** 2884
32. Dolphin D, Traylor T G and Xie L Y 1997 Polyhaloporphyrins: unusual ligands for metals and metal-catalyzed oxidations *Acc. Chem. Res.* **30** 251
33. Fujii H 1993 Effects of the electron-withdrawing power of substituents on the electronic structure and reactivity in oxoiron(IV) porphyrin pi-cation radical complexes *J. Am. Chem. Soc.* **115** 4641
34. Gross Z and Nimri S 1994 A pronounced axial ligand effect on the reactivity of oxoiron(IV) porphyrin cation radicals *Inorg. Chem.* **33** 1731
35. Kumar D, Sastry G N and de Visser S P 2011 Effect of the axial ligand on substrate sulfoxidation mediated by iron(IV)–oxo porphyrin cation radical oxidants *Chem. Eur. J.* **17** 6196
36. Ye S, Geng C Y, Shaik S and Neese F 2013 Electronic structure analysis of multistate reactivity in transition metal catalyzed reactions: the case of C-H bond activation by non-heme iron(IV)–oxo cores *Phys. Chem. Chem. Phys.* **15** 8017
37. Mukherjee G, Alili A, Barman P, Kumar D, Sastri C V and de Visser S P 2019 Interplay between steric and electronic effects: A joint spectroscopy and computational study of nonheme iron(IV)-oxo complexes *Chem. Eur. J.* **25** 5086
38. Jackson T A, Rohde J U, Seo M S, Sastri C V, DeHont R, Stubna A, et al. 2008 Axial ligand effects on the geometric and electronic structure of non-heme oxoiron(IV) complexes *J. Am. Chem. Soc.* **130** 12394
39. Kumar S, Faponle A S, Barman P, Vardhaman A K, Sastri C V, Kumar D and de Visser S P 2014 Long-range electron transfer triggers mechanistic differences between iron(IV)-oxo and iron(IV)-imido oxidants *J. Am. Chem. Soc.* **136** 17102
40. Ahmed M, Khanna S and Bharatam P V 2005 Importance of sulfoxidation in rapid racemisation of glitazones *Ind. J. Chem.* **44B** 600
41. Taxak N, Parmar V, Patel D S, Kotasthane A and Bharatam P V 2011 S-oxidation of thiazolidinedione with hydrogen peroxide, peroxynitrous acid, and C4a-hydroperoxyflavin: a theoretical study *J. Phys. Chem. A* **115** 891
42. Taxak N, Dixit V A and Bharatam P V 2012 Density functional study on the cytochrome-mediated S-oxidation: identification of crucial reactive intermediate on the metabolic path of thiazolidinediones *J. Phys. Chem. A* **116** 10441
43. Sastri C V, Seo M S, Park M J, Kim K M and Nam W 2005 Formation, stability, and reactivity of a mononuclear non-heme oxoiron(IV) complex in aqueous solution *Chem. Commun.* **11** 1405
44. Vardhaman A K, Barman P, Kumar S, Sastri C V, Kumar D and de Visser S P 2013 Comparison of the reactivity of nonheme iron(IV)-oxo versus iron(IV)-imido complexes: Which is the better oxidant? *Angew. Chem. Int. Ed.* **52** 12288
45. Mukherjee G, Cantú Reinhard F G, Bagha U K, Sastri C V and de Visser S P 2020 Sluggish reactivity by a nonheme iron(IV)-tosylimido complex as compared to its oxo analogue *Dalton Trans.* **49** 5921
46. Cantú Reinhard F G, Faponle A S and de Visser S P 2016 Substrate sulfoxidation by an iron(IV)-oxo Complex: Benchmarking computationally calculated barrier heights to experiment *J. Phys. Chem. A* **120** 9805
47. Park J, Morimoto Y, Lee Y M, Nam W and Fukuzumi S 2011 Metal ion effect on the switch of mechanism from direct oxygen transfer to metal ion-coupled electron transfer in the sulfoxidation of thioanisoles by a non-heme iron(IV)-oxo complex *J. Am. Chem. Soc.* **133** 5236
48. Park J, Morimoto Y, Lee Y M, Nam W and Fukuzumi S 2014 Unified view of oxidative C−H bond cleavage and sulfoxidation by a non-heme iron(IV)−oxo complex via lewis acid-promoted electron transfer *Inorg. Chem.* **53** 3618
49. Park M J, Lee J, Suh Y, Kim J and Nam W 2006 Reactivities of mononuclear non-heme iron intermediates including evidence that iron(III)-hydroperoxo species Is a sluggish oxidant *J. Am. Chem. Soc.* **128** 2630
50. İşci Ü, Faponle A S, Afanasiev P, Albrieux F, Briois V, Ahsen V, et al. 2015 Site-selective formation of an iron(IV)-oxo species at the more electron-rich iron atom of heteroleptic μ-nitrido diiron phthalocyanines *Chem. Sci.* **6** 5063
51. Quesne M G, Senthilnathan D, Singh D, Kumar D, Maldivi P, Sorokin A B and de Visser S P 2016 Origin of the enhanced reactivity of μ-nitrido-bridged diiron(IV)-oxo porphyrinoid complexes over cytochrome P450 Compound I *ACS Catal.* **6** 2230
52. Mubarak M Q E, Sorokin A B and de Visser S P 2019 Properties and reactivity of μ-nitrido bridged dimetal porphyrinoid complexes. How does ruthenium compare to iron? *J. Biol. Inorg. Chem.* **24** 1127
53. de Visser S P 2006 Substitution of hydrogen by deuterium changes the regioselectivity of ethylbenzene hydroxylation by an oxo-iron-porphyrin catalyst *Chem. Eur. J.* **12** 8168
54. Cantú Reinhard F G, Sainna M A, Upadhyay P, Balan G A, Kumar D, Fornarini S, et al. 2016 A systematic account on aromatic hydroxylation by a cytochrome P450 model Compound I: A low-pressure mass spectrometry and computational study *Chem. Eur. J.* **22** 18608
55. Louka S, Barry S M, Heyes D J, Mubarak M Q E, Ali H S, Alkhalaf L M, et al. 2020 The catalytic mechanism of aromatic nitration by cytochrome P450 TxtE: Involvement of a ferric-peroxynitrite intermediate *J. Am. Chem. Soc.* **142** 15764
56. *Gaussian* 09, Revision D.01, Frisch M J, Trucks G W, Schlegel H B, Scuseria G E, Robb M A, Cheeseman J R, Scalmani G, Barone V, Mennucci B, Petersson G A,

Nakatsuji H, Caricato M, Li X, Hratchian H P, Izmaylov A F, Bloino J, Zheng G, Sonnenberg J L, Hada M, Ehara M, Toyota K, Fukuda R, Hasegawa J, Ishida M, Nakajima T, Honda Y, Kitao O, Nakai H, Vreven T, Montgomery Jr, J A, Peralta J E, Ogliaro F, Bearpark M, Heyd J J, Brothers E, Kudin K N, Staroverov V N, Keith T, Kobayashi R, Normand J, Raghavachari K, Rendell A, Burant J C, Iyengar S S, Tomasi J, Cossi M, Rega N, Millam J M, Klene M, Knox J E, Cross J B, Bakken V, Adamo C, Jaramillo J, Gomperts R, Stratmann R E, Yazyev O, Austin A J, Cammi R, Pomelli C, Ochterski J W, Martin R L, Morokuma K, Zakrzewski V G, Voth G A, Salvador P, Dannen-berg J J, Dapprich S, Daniels A D, Farkas O, Foresman J B, Ortiz J V, Cioslowski J, Fox D J. Gaussian, Inc., Wallingford CT, 2010.

57. Becke A D 1993 Density-functional thermochemistry. III. The role of exact exchange *J. Chem. Phys.* **98** 5648
58. Lee C, Yang W and Parr R G 1988 Development of the Colle-Salvetti correlation-energy formula into a functional of the electron density *Phys. Rev. B* **37** 785
59. Hay P J and Wadt W R 1985 Ab initio effective core potentials for molecular calculations. Potentials for the transition metal atoms Sc to Hg *J. Chem. Phys.* **82** 270
60. Petersson G A, Bennett A, Tensfeldt T G, Al-Laham M A, Shirley W A and Mantzaris J 1988 A complete basis set model chemistry. I. The total energies of closed-shell atoms and hydrides of the first-row atoms *J. Chem. Phys.* **89** 2193
61. Petersson G A and Al-Laham M A 1991 A complete basis set model chemistry. II. Open-shell systems and the total energies of the first-row atoms *J. Chem. Phys.* **94** 6081
62. Barman P, Upadhyay P, Faponle A S, Kumar J, Nag S S, Kumar D, et al. 2016 Deformylation reaction by a nonheme manganese(III)-peroxo complex via initial hydrogen atom abstraction *Angew. Chem. Int. Ed.* **55** 11091
63. Cummins D C, Alvarado J G, Zaragoza J P T, Mubarak M Q E, Lin Y-T, de Visser S P and Goldberg D P 2020 Hydroxyl transfer to carbon radicals by Mn(OH) versus Fe(OH) corrole complexes *Inorg. Chem.* **59** 16053
64. Pattanayak S, Cantú Reinhard F G, Rana A, Gupta S S and de Visser S P 2019 The equatorial ligand effect on the properties and reactivity of iron(V)-oxo intermediates *Chem. Eur. J.* **25** 8092
65. Barman P, Cantú Reinhard F G, Bagha U K, Kumar D, Sastri C V and de Visser S P 2019 Hydrogen by deuterium substitution in an aldehyde tunes the regioselectivity by a nonheme manganese(III)-peroxo complex *Angew. Chem. Int. Ed.* **58** 10639
66. Timmins A, Saint-André M and de Visser S P 2017 Understanding how prolyl-4-hydroxylase structure steers a ferryl oxidant toward scission of a strong C-H bond *J. Am. Chem. Soc.* **139** 9855
67. Colomban C, Tobing A H, Mukherjee G, Sastri C V, Sorokin A B and de Visser S P 2019 Mechanism of oxidative activation of fluorinated aromatic compounds by N-bridged diiron-phthalocyanine. What determines the reactivity? *Chem. Eur. J.* **25** 14320
68. Ghafoor S, Mansha A and de Visser S P 2019 Selective hydrogen atom abstraction from dihydroflavonol by a nonheme iron center is the key step in the enzymatic flavonol synthesis and avoids byproducts *J. Am. Chem. Soc.* **141** 20278
69. Ali H S, Henchman R H and de Visser S P 2020 Lignin biodegradation by a cytochrome P450 enzyme: A computational study into syringol activation by GcoA *Chem. Eur. J.* **26** 13093
70. Ogliaro F, de Visser S P, Groves J T and Shaik S 2001 Chameleon states: high-valent metal-oxo species of cytochrome P450 and its ruthenium analog *Angew. Chem. Int. Ed.* **40** 2874
71. Green M T 1999 Evidence for sulfur-based radicals in thiolate compound I intermediates *J. Am. Chem. Soc.* **121** 7939
72. Schöneboom J C, Lin H, Reuter N, Thiel W, Cohen S, Ogliaro F and Shaik S 2002 The elusive oxidant species of cytochrome P450 enzymes: characterization by combined quantum mechanical/molecular mechanical (QM/MM) calculations *J. Am. Chem. Soc.* **124** 8142
73. de Visser S P, Shaik S, Sharma P K, Kumar D and Thiel W 2003 Active species of horseradish peroxidase (HRP) and cytochrome P450: two electronic chameleons *J. Am. Chem. Soc.* **125** 15779
74. Bathelt C M, Zurek J, Mulholland A J and Harvey J N 2005 Electronic structure of compound I in human isoforms of cytochrome P450 from QM/MM modelling *J. Am. Chem. Soc.* **127** 12900
75. de Visser S P and Tan L S 2008 Is the bound substrate in nitric oxide synthase protonated or neutral and what is the active oxidant that performs substrate hydroxylation? *J. Am. Chem. Soc.* **130** 12961
76. Li D, Wang Y, Han K and Zhan C-G 2010 Fundamental reaction pathways for cytochrome P450-catalyzed 5′-hydroxylation and N-demethylation of nicotine *J. Phys. Chem. B* **114** 9023
77. Hirao H, Chuanprasit P, Cheong Y Y and Wang X 2013 How is a metabolic intermediate formed in the mechanism-based inactivation of cytochrome P450 by using 1,1-dimethylhydrazine: Hydrogen abstraction or nitrogen oxidation? *Chem. Eur. J.* **19** 7361
78. Lai R and Li H 2016 Hydrogen abstraction of camphor catalyzed by cytochrome P450cam: A QM/MM study *J. Phys. Chem. B* **120** 12312
79. Phung Q M and Pierloot K 2019 Low-lying electromeric states in chloro-ligated iron(IV)-oxo porphyrin as a model for compound I, studied with second-order perturbation theory based on density matrix renormalization group *J. Chem. Theory Comput.* **15** 3033
80. Sainna M A, Kumar S, Kumar D, Fornarini S, Crestoni M E and de Visser S P 2015 A comprehensive test set of epoxidation rate constants by iron(IV)-oxo porphyrin complexes *Chem. Sci.* **6** 1516
81. Bernadou J and Meunier B 1998 'Oxo-hydroxo tautomerism' as useful mechanistic tool in oxygenation reactions catalysed by water-soluble metalloporphyrins *Chem. Commun.* **20** 2167
82. Rohde J U, In J H, Lim M H, Brennessel W W, Bukowski M R, Stubna A, et al. 2003 Crystallographic

and spectroscopic characterization of a nonheme Fe(IV)=O Complex *Science* **299** 1037
83. Nam W 2007 High-valent iron(IV)–oxo complexes of heme and non-heme ligands in oxygenation reactions *Acc. Chem. Res.* **40** 522
84. Ghosh S K, Patra R and Rath S P 2010 Synthesis and characterization of *anti*-bis Fe(III) porphyrins, *syn*-bis Fe(III)-μ-oxo porphyrin, and *syn*-bis Fe(III)-μ-oxo porphyrin cation radical *Inorg. Chem.* **49** 3449
85. Hohenberger J, Ray K and Meyer K 2012 The biology and chemistry of high-valent iron oxo and iron–nitrido complexes *Nat. Commun.* **3** 720
86. Fuji H 2002 Electronic structure and reactivity of high-valent oxo iron porphyrins *Coord. Chem. Rev.* **226** 51
87. Ghosh A 1998 First-principles quantum chemical studies of porphyrins *Acc. Chem. Res.* **31** 189
88. Shaik S, Lai W, Chen H and Wang Y 2010 The valence bond way: reactivity patterns of cytochrome P450 enzymes and synthetic analogs *Acc. Chem. Res.* **43** 1154
89. Prokop K A, Neu H M, de Visser S P and Goldberg D P 2011 A manganese(V)-oxo π-cation radical complex: Influence of one-electron oxidation on oxygen-atom transfer *J. Am. Chem. Soc.* **133** 15874
90. Kumar D, de Visser S P, Sharma P K, Hirao H and Shaik S 2005 Sulfoxidation mechanisms catalyzed by cytochrome P450 and horseradish peroxidase models: spin selection induced by the ligand *Biochemistry* **44** 8148
91. Hansch C, Leo A and Taft R W 1991 A survey of hammett substituent constants and resonance and field parameters *Chem. Rev.* **91** 165
92. Mukherjee G, Lee C W Z, Nag S S, Cantú Reinhard F G, Kumar D, Sastri C V and de Visser S P 2018 Dramatic rate-enhancement of oxygen atom transfer by an iron(IV)-oxo species by equatorial ligand field perturbations *Dalton Trans.* **47** 14945
93. Cantú Reinhard F G, Barman P, Mukherjee G, Kumar J, Kumar D, Kumar D, et al. 2017 Keto-enol tautomerization triggers an electrophilic aldehyde deformylation reaction by a nonheme manganese(III)-peroxo complex *J. Am. Chem. Soc.* **139** 18328
94. Kumar D, Latifi R, Kumar S, Rybak-Akimova E V, Sainna M A and de Visser S P 2013 Rationalization of the barrier height for para-Z-styrene epoxidation by iron(IV)-oxo porphyrins with variable axial ligands *Inorg. Chem.* **52** 7968
95. Sharma P K, de Visser S P and Shaik S 2003 Can a single oxidant with two spin states masquerade as two different oxidants? A study of the sulfoxidation mechanism by cytochrome P450 *J. Am. Chem. Soc.* **125** 8698
96. Shaik S, Kumar D and de Visser S P 2008 A valence bond modeling of trends in hydrogen abstraction barriers and transition states of hydroxylation reactions catalyzed by cytochrome P450 enzymes *J. Am. Chem. Soc.* **130** 10128
97. de Visser S P 2010 Trends in substrate hydroxylation reactions by heme and nonheme iron(IV)-oxo oxidants give correlations between intrinsic properties of the oxidant with barrier height *J. Am. Chem. Soc.* **132** 1087
98. Kumar D, Karamzadeh B, Sastry G N and de Visser S P 2010 What factors influence the rate constant of substrate epoxidation by Compound I of cytochrome P450 and analogous iron(IV)-oxo oxidants *J. Am. Chem. Soc.* **132** 7656
99. Lias S G 2009 Ionization energy evaluation. In NIST Chemistry Webbook, NIST Standard Reference Database Number 69, Linstrom P J and Mallard W G (Eds.), National Institute of Standards and Technology, Gaithersburg MD, 20899. http://webbook.nist.gov
100. Friedrich L E 1983 The two hydrogen-oxygen bond-dissociation energies of hydroquinone *J. Org. Chem.* **48** 3851
101. Bordwell F G and Cheng J-P 1991 Substituent effects on the stabilities of phenoxyl radicals and the acidities of phenoxyl radical *J. Am. Chem. Soc.* **113** 1736
102. Mayer J M 2004 Proton-coupled electron transfer: A reaction chemist's view *Annu. Rev. Phys. Chem.* **55** 363
103. Ali H S, Henchman R H, Warwicker J and de Visser S P 2021 How do electrostatic perturbations of the protein affect the bifurcation pathways of substrate hydroxylation versus desaturation in the nonheme iron-dependent viomycin biosynthesis enzyme? *J. Phys. Chem. A* **125** 1720
104. Ali H S, Henchman R H and de Visser S P 2021 What determines the selectivity of arginine dihydroxylation by the nonheme iron enzyme OrfP? *Chem. Eur. J.* **27** 1795